

Design and Modeling of an Extensible Soft Robotic Arm

Xiaojiao Chen¹, *Student Member, IEEE*, Yaoxin Guo¹, Dehao Duanmu¹, Jianshu Zhou¹, *Student Member, IEEE*, Wei Zhang², *Senior Member, IEEE* and Zheng Wang^{1,2,*}, *Senior Member, IEEE*

Abstract—Soft robotic arms are receiving more and more attention for their intrinsic safety and natural compliance. Instead of traditional serialized rotary joints, soft robotic arms often have complex joints with coupled degrees of freedom like bending, rotation and elongation, enabling them with more freedoms in achieving sophisticated movements. However, currently soft robotic arms are mostly focusing on bending and rotation, while elongation is either unavailable due to the inextensible backbone or only has a small range because of the limited contraction ratio of actuators. Furthermore, the coupling of actuators and complex structure makes the modeling and control hard. In this paper, we introduced an extensible soft robotic arm with a large elongation ratio of 400%, and give a novel modeling method from a new perspective of the force balance of the arm. The models were experimentally tested both in loaded and unloaded situations, showing the effectiveness of predicting the bending, rotation and elongation of the arm.

Index Terms—Modeling, Control, and Learning for Soft Robots, Soft Robot Applications, Kinematics.

I. INTRODUCTION

SOFT robotic arms, are naturally safe by using soft materials and structures [1]–[5]. Their natural compliance empowers them with excellent adaptation to deal with uncertainty and disturbance, allowing for low cost safe and pleasant human-robot interaction [6]–[11].

For decades, the efforts of developing a soft robotic arm have never stopped. In general, most of the soft robotic arms could be regarded as combinations of tendons, springs, pneumatic actuators and backbones [12], [13]. Back-bones [14] are the easy choice for their stable structure, such as the Arm Orm [15] and the Tensor arm [16], Active Hose [17], omni-thread serpentine robot [18] and Elephant Trunk Robot [19]. However, back-boned soft robotic arms often suffer from

the limited bending angle of one segment and are incapable of changing their length freely. For the non-backbone robotic arms, the soft arms are either supported by elastic silicon rubber chambers or extensible pneumatic actuators, therefore the overall length could be altered to some degree. For example, Octopus arm in [20], [21] uses tendons to alter the cross section area to generate the elongation movement. Some soft robotic arms use partially constrained silicon chambers, such as the flexible micro actuator [22], Air-ocor [23], COLOBOT [24], STIFF-SLOP manipulator [25]. These two kinds of soft arms only have small freedom to change the length because of structural and material limitations. Pneumatic Artificial Muscle(PAM) are also widely used, such as the OctArm in [26], [27] and [28], [29]. Although the length could be changed more, the elongation ratio is still less than 80% or contraction ratio less than 40% because of the limitation of PAM. They also suffer from dramatically decreasing output force when away from the original length, greatly complicating the design and control.

Bellow-based robotic arms, such as KSI Tentacle manipulator in [30], Slim Slime Robot in [31], Bionic Handling Assistant [32] and Bionic Motion Robot [33], are either combing additional tendons or springs which greatly complicated the overall system, or using specially fabricated bellows which are not easily accessible. Meanwhile, these soft arms are more focusing on the bending and rotation, not the elongation part. Some recent studies have shown more systematical ways for developing bellow typed arms, such as in [34] and [35] who used 3D-printing to accelerate the designing and fabricating process, or in [36] who designed a novel sensor for this kind of arm.

The modeling and control of bellow based arms are often complex and hard to implement [37]. Previous models are mostly from the geometric point of view, commonly based on the assumption of constant curvatures [12], studying the kinematics relationship of the arm's actuator length and the final posture, requiring great efforts to design and install different sensors like length encoders, IMUs, vision systems. However, for some applications, the compliance of the soft arm makes the accuracy of the position less important. Sometimes a good model capable of predicting the motion of the arm could achieve the desired goal without complex feedback sensors.

In this paper, we introduced an extensible soft robotic arm (ExtenSA) that has a large elongation ratio of 400%. A novel modeling method of this arm based on the force balance of the ending plate was derived and given in a general form. Experiments showed that the model could predict the actual

Manuscript received: February, 24, 2019; Revised May, 5, 2019; Accepted July, 1, 2019.

This paper was recommended for publication by Editor Cho, Kyu-Jin upon evaluation of the Associate Editor and Reviewers' comments. The presented research has been supported by Hong Kong RGC-ECS Grant 27210315, ITF Grant ITS/140/18 and IT457/17FP, HKU Seed Funding 201611159196, 201611160034, 201711160023, and 201711159158.

¹X. Chen, Y. Guo, D. Dehao, Z. Zhou and Z. Wang are with the Department of Mechanical Engineering, the University of Hong Kong, Hong Kong SAR, China, chen2014@connect.hku.hk, grace11.1@foxmail.com, bitduanmu@126.com, zhoujs@connect.hku.hk, zwangski@hku.hk.

²W. Zhang and Z. Wang are also with the Department of Mechanical and Energy Engineering, Southern University of Science and Technology, China, zhangw3@sustech.edu.cn, wangz@sustech.edu.cn.

*Corresponding author: Zheng Wang. Tel: +852-3917-7905, Fax: +852-2858-5415. zwangski@hku.hk.

Digital Object Identifier (DOI): see top of this page.

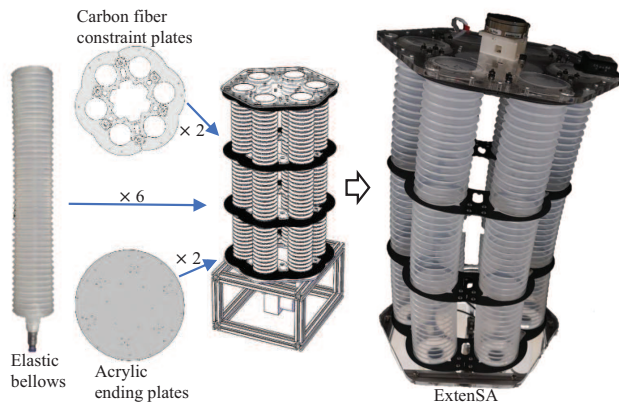


Fig. 1. The ExtenSA is composed of 6 long bellows, two ending plates and intermediate carbon fiber supporting plates. As a backbone-less soft arm, the structure of ExtenSA is stable due to the large cross section area of the bellows and the installation payload distance between bellows. ExtenSA weights only 800g, but has a large payload of more than 20kg vertically.

state both in loaded and unloaded situations, promising for sensor-less applications or advanced controls.

The originality of this paper includes:

- 1) We introduced a light-weight extensible soft robotic arm ExtenSA with large elongation ratio and large payload.
- 2) A novel modeling method for bending, rotation and elongation were given in a general form, both in loaded and unloaded situations and experimentally testified.

In section II, the design of the ExtenSA was given. In section III, the modeling of elongation, bending and rotation are derived, followed by the experimental validation individually in loaded and unloaded situations in section IV.

II. DESIGN

A. Design of ExtenSA

The ExtenSA is a light-weight backbone-less soft robotic arm, consisting of 6 long elastic bellows installed circularly between two acrylic plates, as shown in Fig. 1. The bellows are vertically glued onto the acrylic plates, which is essential for the transmission of force. The parameters of the ExtenSA are listed in Table. I.

The bellows are evenly distributed around the center by an angle of 60° . The arm is totally supported by the 6 bellows, without any other tendons or backbones for support. The hollow inside the bellows group could be used to pass through tubes or other tools.

One common problem in utilizing bellows is their tendency to buckle under large payloads. Previous designs mostly use short bellows forming small segments for stacking to a larger soft robotic arm, which is complex and the bending angle of one segment is limited because of the short length of the actuators. In our design, long bellows are used to achieve a large bending angle in just one segment. Two thin carbon fiber plates were added in the middle, constraining the relative radial movement of the bellows on that plane as shown in Fig. 2. The large elongation ratio fulfills ExtenSA a large workspace in different bending configurations as shown in Fig. 3.



Fig. 2. The length of ExtenSA could reach from 100mm to 500mm, with a maximum elongation ratio of 400%. The bending angle of ExtenSA is 100° , and the payload of ExtenSA could reach more than 20kg vertically.

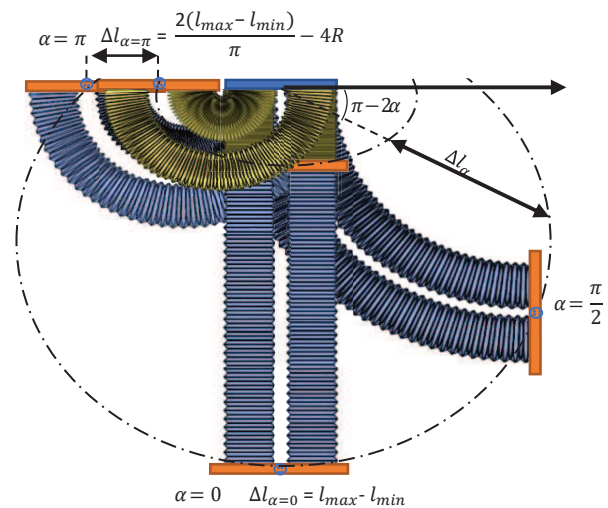


Fig. 3. The geometric representation of the available freedom to move under a certain bending angle α .

As a backbone-less soft robotic arm, the ExtenSA has a relatively large stiffness due to the structural distribution of the 6 bellows. The installation distances between the bellows are large, compared to other soft robotic arms, providing a large lever-arm to sustain its bending posture. This enables ExtenSA to have a stable output while maintaining safe compliance.

B. Comparison With Other Soft Robotic Arms

Compared with PAM-based soft robotic arm, ExtenSA has a much larger ratio which reaches 400%. PAMs only have a contraction ratio of less than 40% or an elongation ratio less than 80%. The PAM works at a relative high pressure source, while ExtenSA has a larger effective area and a lower working pressure.

TABLE I
PARAMETERS OF EXTENSA

bellows number	radius	minimal length	maximum length	maximum elongation ratio	bending angle(α)	rotation angle(β)	weight	working pressure	vertical payload	horizontal payload
6	0.11m	0.1m	0.5m	400%	(0°, 100°)	(0°, 360°)	800g	(-100kPa, 200kPa)	20kg	5kg

Compared with other bellow-based soft arms as in [34], [36] who used 3 and 4 relatively short bellows, ExtenSA uses 6 long bellows (500mm) to form an entire arm. Unlike [36] that has a backbone supporting the arm, resisting large length changes, our ExtenSA is supported by 6 stretchable bellows allowing for a large extension. Similar to [34] we tackled the problem of buckling by adding carbon fiber plates, avoiding the complex segmentation as shown in Fig. 2. But we are using much larger and longer bellows that could deal with larger payloads and longer elongation ratio of more than 400%.

III. MODELING

A. Modeling of Length

The output force of bellows could be regarded as a combination of the pressure force and the spring force of bellows. The pressure force roughly grows linearly with the pressure inputs. The slope is determined by the effective area, which is slightly changing in our case. The spring effect of bellows is related to the materials and shapes. In this paper, we used an experimental model for the bellows as in [38], and a linear spring force model was used accordingly for simplicity. This assumption holds when the bellows are not near their extreme positions. Finally, the total output force along the normal direction of the plate can be written as

$$F = \sum_{i=1}^N [P_i A - k(l_i - l_0)] \quad (1)$$

where i represents the i 'th chamber, F is the output force, P is the internal gauge pressure inside bellows, A is the effective area of the cross-section of bellows, k is the spring coefficient of one bellow, l_i is the length of the i 'th centerline, l_0 is the initial length.

As shown in Fig. 4(a), the individual centerline length l_i has a relationship with the centerline of the overall arm l_m by

$$l_i = \left[\frac{l_m}{\alpha} - R \cos(\theta_i - \beta) \right] \alpha = l_m - \alpha R \cos(\theta_i - \beta) \quad (2)$$

where R is the installation radius of the bellows, θ_i is the installation angle of individual bellows with respect to the X axis, α is the bending angle illustrated in Fig. 4(c), and β is the rotation angle illustrated in Fig. 4(b). Therefore, we could obtain,

$$\sum_{i=1}^N l_i = N l_m - \alpha R \sum_{i=1}^N \cos(\theta_i - \beta) = N l_m \quad (3)$$

and the total output force equation could be further reduced into

$$F = A \Phi_p - N k (l_m - l_0) \quad (4)$$

where

$$\Phi_p \stackrel{\text{def}}{=} \sum_{i=1}^N P_i \quad (5)$$

This equation describes the force balance along the extension direction.

B. Modeling of Rotation Movement

The rotation movement is described as the angle between the bending plane and the X-Z plane. In free moving situations, this requires the torque generated by all the bellows around the \vec{N}_β as shown in Fig. 4(b) to be zero. The torque output regarding \vec{N}_β is

$$T_{ext}^\beta = \sum_{i=1}^N [F_i R \sin(\theta_i - \beta)]. \quad (6)$$

Substituting (2) into (6), we get

$$T_{ext}^\beta = \sum_{i=1}^N [(P_i A + k(l_m - l_0) - k \alpha R \cos(\theta_i - \beta)) R \sin(\theta_i - \beta)] \quad (7)$$

Considering the following equations which always hold if N actuation units are uniformly distributed circularly, that is with $\theta_i = \frac{i}{N} 2\pi$,

$$\sum_{i=1}^N \sin(\theta_i - \beta) = 0$$

and

$$\sum_{i=1}^N [\cos(\theta_i - \beta) \sin(\theta_i - \beta)] = 0,$$

the last two terms in (7) become zero.

Therefore, the final torque equation regarding β is

$$\begin{aligned} T_{ext}^\beta &= AR \sum_{i=1}^N [P_i \sin(\theta_i - \beta)] \\ &= AR \begin{bmatrix} -\Phi_c & \Phi_s \end{bmatrix} \begin{bmatrix} \sin \beta \\ \cos \beta \end{bmatrix} \end{aligned} \quad (8)$$

where we define

$$\Phi_c \stackrel{\text{def}}{=} \sum_{i=1}^N [P_i \cos \theta_i] \quad (9)$$

and

$$\Phi_s \stackrel{\text{def}}{=} \sum_{i=1}^N [P_i \sin \theta_i] \quad (10)$$

Thus, we get the equation of describing the rotation motion written as

$$\begin{bmatrix} -\Phi_c & \Phi_s \end{bmatrix} \begin{bmatrix} \sin \beta \\ \cos \beta \end{bmatrix} = \frac{T_{ext}^\beta}{AR} \quad (11)$$

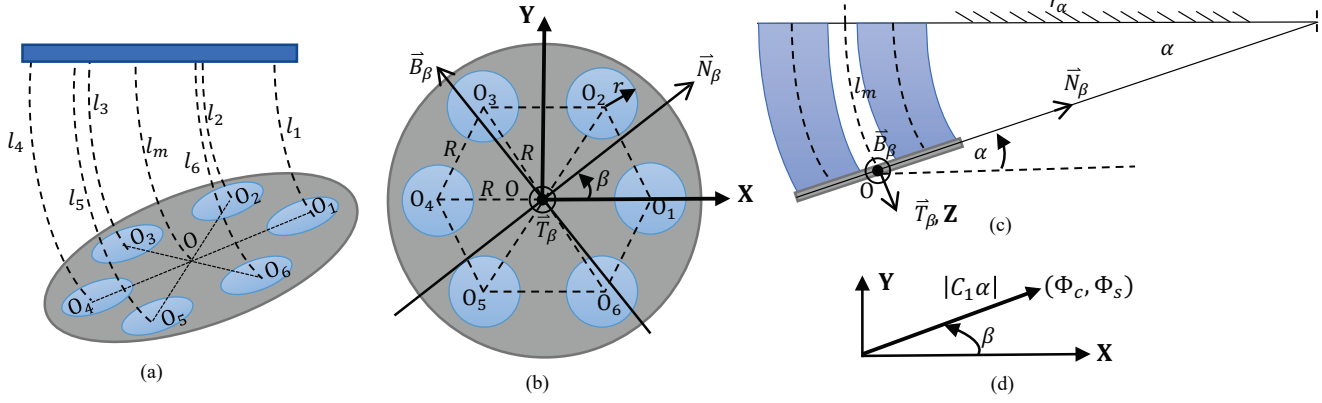


Fig. 4. Geometric representations of ExtenSA.

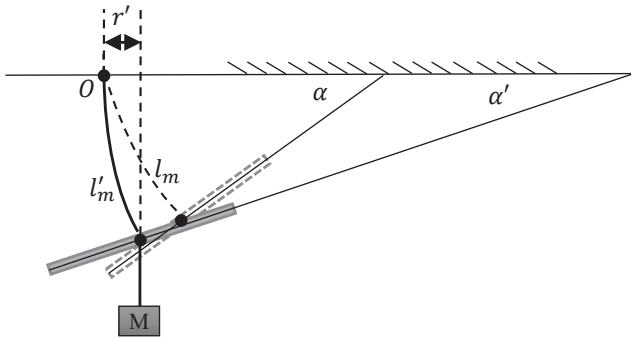


Fig. 5. The external load would exert a bending torque around the center fixing point of the arm as well as a pulling force along the centerline of the arm, affecting the bending angle α and the length l_m .

C. Modeling of Bending Movement

Similarly, the torque output for bending movement is given by

$$T_{ext}^{\alpha} = \sum_{i=1}^N [F_i R \cos(\theta_i - \beta)] \quad (12)$$

Substituting (2) into (12), we get

$$T_{ext}^{\alpha} = \sum_{i=1}^N [(P_i A - k(l_m - l_0) + k\alpha R \cos(\theta_i - \beta)) R \cos(\theta_i - \beta)] \quad (13)$$

with

$$\sum_{i=1}^N \cos(\theta_i - \beta) = 0$$

and

$$\sum_{i=1}^N \cos^2(\theta_i - \beta) = \frac{N}{2},$$

The final general torque equations regarding α can be written as

$$\begin{aligned} T_{ext}^{\alpha} &= AR \sum_{i=1}^N [P_i \cos(\theta_i - \beta)] + \frac{NkR^2\alpha}{2} \\ &= AR [\Phi_s \quad \Phi_c] \begin{bmatrix} \sin \beta \\ \cos \beta \end{bmatrix} + \frac{Nk\alpha R^2}{2} \end{aligned} \quad (14)$$

Thus, we get the equation

$$[\Phi_s \quad \Phi_c] \begin{bmatrix} \sin \beta \\ \cos \beta \end{bmatrix} = \frac{T_{ext}^{\alpha}}{AR} - C_1\alpha \quad (15)$$

where

$$C_1 = \frac{NkR}{2A}$$

D. Modeling Result

Combing (4), (11), and (15), we obtain the following equation group,

$$\begin{bmatrix} \cos \beta & \sin \beta & 0 \\ -\sin \beta & \cos \beta & 0 \\ 0 & 0 & 1 \end{bmatrix} \begin{bmatrix} \Phi_c \\ \Phi_s \\ \Phi_p \end{bmatrix} = \begin{bmatrix} \frac{T_{ext}^{\alpha}}{AR} - C_1\alpha \\ \frac{T_{ext}^{\beta}}{AR} \\ \frac{F + Nk(l_m - l_0)}{AR} \end{bmatrix} \quad (16)$$

which leads to the following solution:

$$\begin{bmatrix} \alpha \\ \beta \\ l_m \end{bmatrix} = \begin{bmatrix} \frac{\frac{T_{ext}^{\alpha}}{AR} - \sqrt{\Phi_c^2 + \Phi_s^2} - (\frac{T_{ext}^{\beta}}{AR})^2}{C_1}} \\ atan2(\Phi_s, \Phi_c) - atan2(\frac{T_{ext}^{\beta}}{AR}, \frac{T_{ext}^{\alpha}}{AR} - C_1\alpha) \\ \frac{A\Phi_p - F}{Nk} + l_0 \end{bmatrix} \quad (17)$$

When the external load is zero, the result could be simplified as

$$\begin{bmatrix} \alpha \\ \beta \\ l_m \end{bmatrix} = \begin{bmatrix} \frac{\sqrt{\Phi_c^2 + \Phi_s^2}}{C_1} \\ atan2(\Phi_s, \Phi_c) - \pi \\ \frac{R\Phi_p}{2C_1} + l_0 \end{bmatrix} \quad (18)$$

This model could be used to guide the design of the arm. For example from (18) we could see that the bending angle α has a linear relationship with the effective area of the bellows but an inverse relationship with the installation radius R , which indicates that it would be more effective to reduce the installation radius in order to achieve large bending angle.

It could also be used to predict the configuration of the arm under certain pressure commands, eliminating the usage of posture sensors, and enabling applications where high precision is not required and sensors are hard to acquire or install.

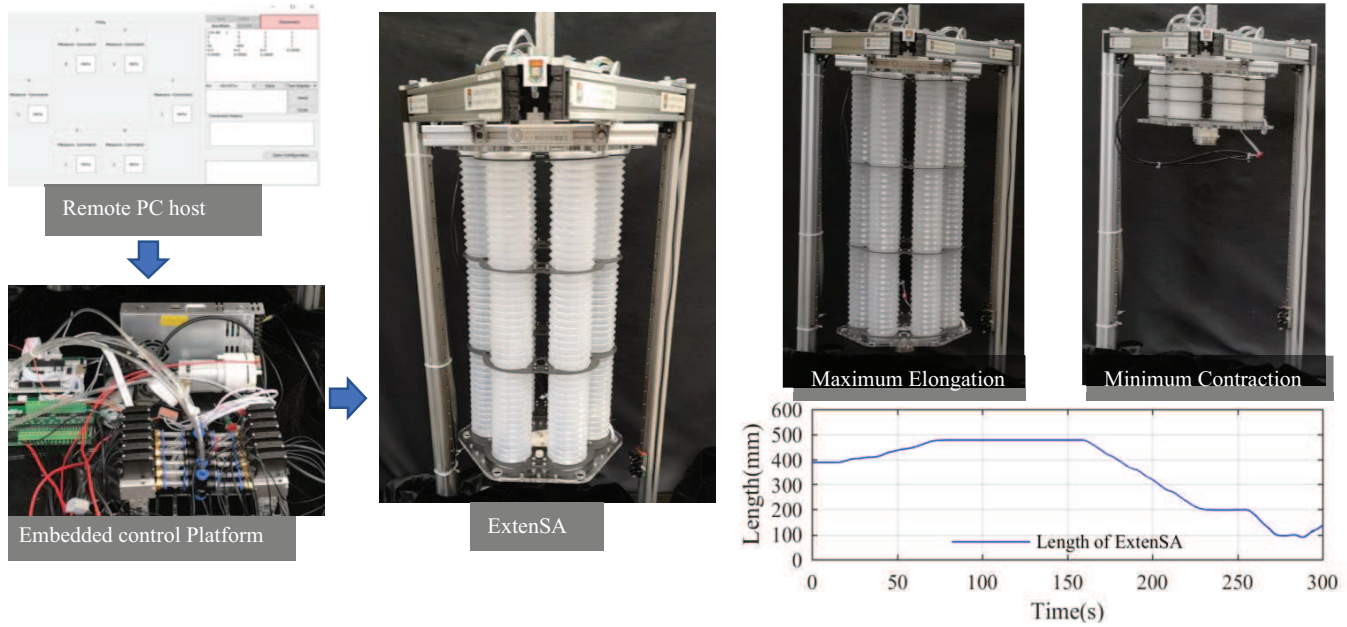


Fig. 6. The experimental setup and demonstration of the elongation limits of ExtenSA.

E. Modeling With External Load

This model also holds when an external load exists. In this paper, we assume the arm is loaded with mass m at the end of the ending plate. From Fig. 5 we could see the mass exerts a bending torque and a pulling force affecting both α and l_m .

By taking the arm from free state to loaded situations, the bending angle would become α' and the length would become l'_m . According to (15), we get the following equation

$$-\frac{Mgl'_m(1 - \cos \alpha')}{AR\alpha'} - c_1\alpha' = -c_1\alpha \quad (19)$$

To simplify the calculation, the approximation of $1 - \cos \alpha' \approx \frac{\alpha'^2}{2}$ and $l'_m \approx l_m$ were applied to obtain α' , leading to

$$\alpha' = \frac{2ARC_1}{2ARC_1 + mgl_m}\alpha \quad (20)$$

The approximation of $\alpha \approx \alpha'$ was used to obtain the l'_m , leading to

$$l'_m = \frac{mg \cos \alpha}{Nk} + l_m \quad (21)$$

These two equations could be used to compensate the change of α and l_m due to external loads.

IV. EXPERIMENTS VALIDATION

In this section we show the effectiveness of the model for predicting the configuration state of the arm both in unloaded and loaded situations. The experimental setup is shown in Fig. 6, where the ExtenSA is inversely installed on a platform. All six bellows have pressure sensors with a gauge range from $-100KPa$ to $300KPa$. A rope encoder is installed along the centerline of the ExtenSA, providing the length feedback of l_m with an accuracy of $1mm$. An IMU is fixed at the center of the plate, with the coordinates coinciding with that of the ExtenSA. The IMU would generate quaternions with

an updating frequency of 50Hz. The measured bending angle α and rotation angle β are acquired from these quaternions.

We first validate the model in unloaded situations, where the arm is not attached to any external weight. Then we show the loaded situations.

A. Length Model Unloaded

To show the elongation ability of ExtenSA, the 6 bellows were first pressurized to reach the arm's maximum length and then vacuumed to reach the minimal length. As seen in Fig. 6, the minimal length reaches below $100mm$, and the largest length goes up to $500mm$, with an elongation ratio of 400% or contraction ratio of 80%.

We validated the length model by freely changing the state of the arm. As shown in Fig. 7(a), the measured length of the centerline could be tracked through our model. During the time $t = 10s$ and $t = 28s$, the tracking error is larger because of the hysteresis and friction of the bellows. The error plot is shown in Fig. 7(d), and the maximum absolute error is $38mm$ and the standard deviation error is $15mm$.

B. Rotation Model Unloaded

We used a joystick to generate the rotation motion without any particular constraints by inflating some bellows and deflating the opposing ones. The predicted value of β was derived through the model equation, and the measured value was acquired by rotating the normal vector of the ending plate with the instant quaternion. As seen from the result in Fig. 7(b), the result shows that the model predicts the rotation movement. The error of the rotation model is shown in Fig. 7(e), with a maximum absolute error of 30° and a standard deviation of 24° .

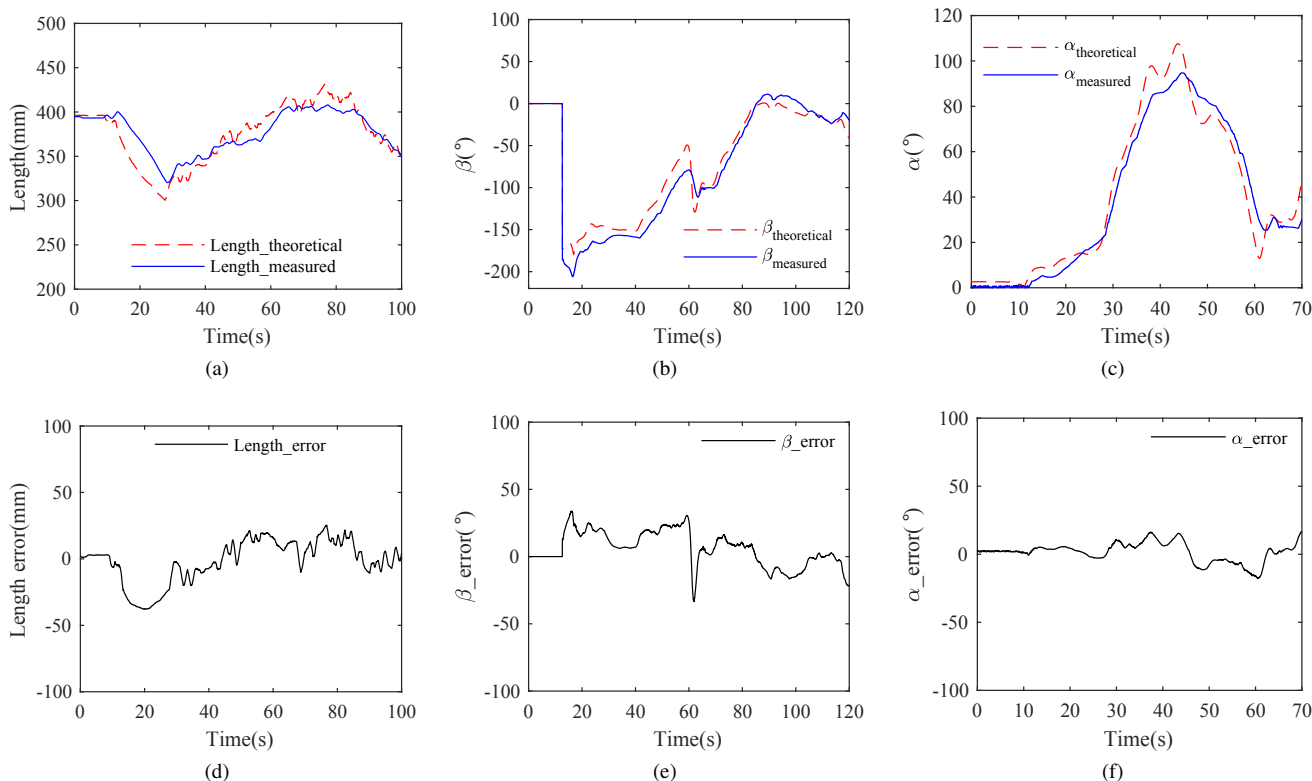


Fig. 7. Predicting performance of the models. (a) The measured length of the centerline of the ExtenSA could be predicted by our model. At time $t = 0s$, the initial length is 392mm. At $t = 10s$, the pressures sums were decreasing, and the ExtenSA started to contract. At $t = 30s$, the pressures started to increase, and the length became longer. (b) The theoretical value of rotation angle β could predict the actual rotation movement. (c) The theoretical value of bending angle α could predict the actual bending movement. (d) Modeling error of l_m . (e) Modeling error of α . (f) Modeling error of β .

C. Bending Model Unloaded

We used a joystick to generate the bending motion as well. The predicted value of α was derived through the model equation, and the measured value was acquired from the instant quaternion. As we could see from Fig. 7(c), the model predicts the actual bending state. The error of the bending modeling is shown in Fig. 7(f), with a maximum absolute error of 17° and a standard deviation of 10° .

D. Simultaneous Tracking Unloaded

Here we show how the three models of length, rotation and bending could simultaneously predict the movement of the ExtenSA.

The movements of the ExtenSA are generated randomly, with different combinations of elongation, rotation and bending. Then the measured data and the theoretical data were plotted in Fig. 8, showing an acceptable tracking ability.

E. Loaded Situations

In this section, we test the effectiveness of the model under external loads.

In the first experiment, the bending angle command was given as a sin wave, with the length and rotation angle command constant. A force and torque sensor was installed at the center of the plate. First the arm was unloaded, then external masses of $0.51Kg$ and $0.9Kg$ were loaded at the force

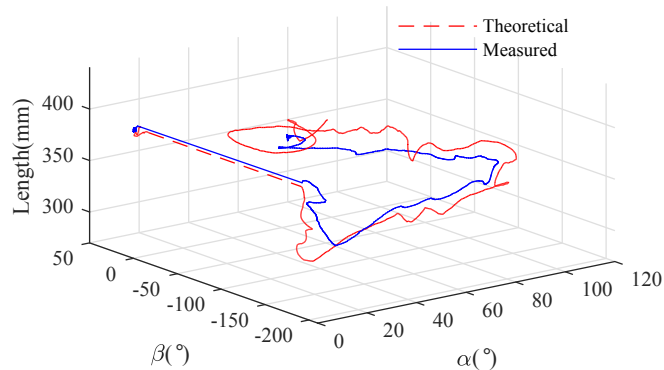


Fig. 8. The complex movement of the ExtenSA, with random postures combining different length, bending angle and rotation angle, could be predicted by our model.

sensor successively, representing the weight of commonly used tools like a screwdriver. This would cause the average bending angle α to decrease. The measured angle and model angle predicted by (20) was plotted in Fig. 9(a), and the average of $\Delta\alpha$ was plotted in Fig. 9(c). The result shows that the external disturbance could be described by the model.

In the second experiment, length was commanded at a constant of $325mm$ with α commanded at $\pi/6$ and β commanded at π . Increasing weights were added at the force sensor, causing the extension of the actual length. The results were

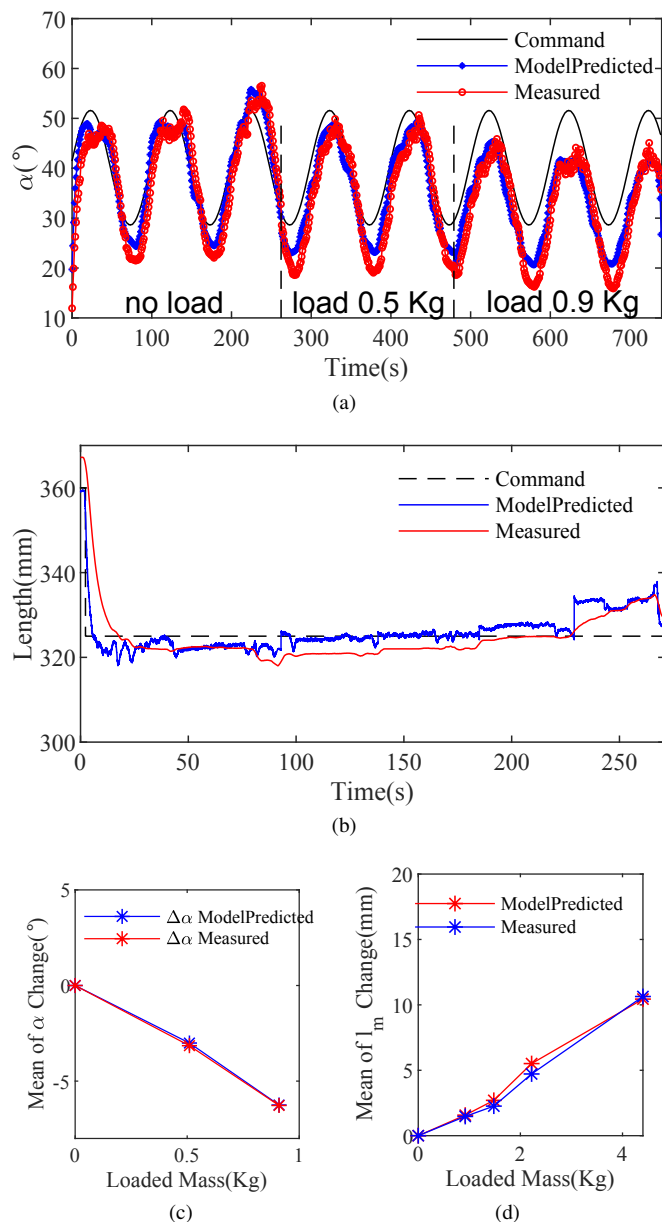


Fig. 9. (a) The bending angle under different external loads. (b) The length under different external loads. (c) The model predicted average change of bending angle α and length l_m

plotted in Fig. 9(b) and 9(d). The modeled length from (21) could predict the change of the measurement.

V. CONCLUSION

In this paper, an extensible soft robotic arm (ExtenSA) was introduced that has a large elongation ratio of more than 400%. A novel method of modeling this type of soft robotic arms was given in a general form, and then experimentally validated. A simultaneous tracking of the length, bending angle, and rotation angle using these models without feedback control is carried out, showing acceptable tracking error, showing the effectiveness of these models to simplify the control. Loaded situations were also studied to show the working capacity of this arm.

In the future, feedback control using this model would be studied to gain better position control performance.

REFERENCES

- [1] J. Yi, X. Chen, C. Song, and Z. Wang, "Fiber-Reinforced Origamic Robotic Actuator," *Soft Robotics*, vol. 5, no. 1, pp. 81–92, 2017.
- [2] J. Yi, X. Chen, and Z. Wang, "A Three-Dimensional-Printed Soft Robotic Glove With Enhanced Ergonomics and Force Capability," *IEEE Robotics and Automation Letters*, vol. 3, no. 1, pp. 242–248, jan 2018.
- [3] J. Zhou, S. Chen, and Z. Wang, "A Soft-Robotic Gripper With Enhanced Object Adaptation and Grasping Reliability," *IEEE Robotics and Automation Letters*, vol. 2, no. 4, pp. 2287–2293, 2017.
- [4] J. Zhou, J. Yi, X. Chen, Z. Liu, and Z. Wang, "BCL-13: A 13-DOF Soft Robotic Hand for Dexterous Grasping and In-Hand Manipulation," *IEEE Robotics and Automation Letters*, vol. 3, no. 4, pp. 3379–3386, oct 2018.
- [5] J. Zhou, X. Chen, J. Li, Y. Tian, and Z. Wang, "A soft robotic approach to robust and dexterous grasping," *2018 IEEE International Conference on Soft Robotics, RoboSoft 2018*, no. 200, pp. 412–417, 2018.
- [6] X. Chen, J. Yi, J. Li, J. Zhou, and Z. Wang, "Soft-actuator-based robotic joint for safe and forceful interaction with controllable impact response," *IEEE Robotics and Automation Letters*, vol. 3, no. 4, pp. 3505–3512, oct 2018.
- [7] J. Yi, X. Chen, C. Song, J. Zhou, Y. Liu, S. Liu, and Z. Wang, "Customizable Three-Dimensional-Printed Origami Soft Robotic Joint With Effective Behavior Shaping for Safe Interactions," *IEEE Transactions on Robotics*, p. (Accepted), 2018.
- [8] Z. Wang, A. Peer, and M. Buss, "An HMM approach to realistic haptic Human-Robot interaction," *Proceedings - 3rd Joint EuroHaptics Conference and Symposium on Haptic Interfaces for Virtual Environment and Teleoperator Systems, World Haptics 2009*, pp. 374–379, 2009.
- [9] Z. Wang, A. Peer, and M. Buss, "Fast online impedance estimation for robot control," in *IEEE 2009 International Conference on Mechatronics, ICM 2009*, 2009.
- [10] Z. Wang, Z. Sun, and S. J. Phee, "Haptic feedback and control of a flexible surgical endoscopic robot," *Computer Methods and Programs in Biomedicine*, vol. 112, no. 2, pp. 260–271, Nov 2013.
- [11] Z. Wang, P. Polygerinos, J. T. Overvelde, K. C. Galloway, K. Bertoldi, and C. J. Walsh, "Interaction Forces of Soft Fiber Reinforced Bending Actuators," *IEEE/ASME Transactions on Mechatronics*, vol. 22, no. 2, pp. 717–727, 2017.
- [12] R. J. Webster and B. A. Jones, "Design and kinematic modeling of constant curvature continuum robots: A review," *International Journal of Robotics Research*, vol. 29, no. 13, pp. 1661–1683, 2010.
- [13] X. Chen, J. Peng, J. Zhou, Y. Chen, M. Y. Wang, and Z. Wang, "A robotic manipulator design with novel soft actuators," in *2017 IEEE International Conference on Robotics and Automation (ICRA)*. IEEE, may 2017, pp. 1878–1884.
- [14] I. D. Walker, "Continuous Backbone "Continuum" Robot Manipulators," *ISRN Robotics*, vol. 2013, pp. 1–19, 2013.
- [15] M. N. Pedersen, *The Robot: The Life Story of a Technology - by Lisa Nocks*. Westport Conn.: Greenwood Press, 2009, vol. 51, no. 4.
- [16] V. C. A. Horn and R. C., *Tensor arm manipulator design*. New York N.Y.: ASME, 1967, vol. 67, no. DE-44.
- [17] H. Tsukagoshi, A. Kitagawa, and M. Segawa, "Active hose: An artificial elephant's nose with maneuverability for rescue operation," *Proceedings - IEEE International Conference on Robotics and Automation*, vol. 3, pp. 2454–2459, 2001.
- [18] J. Borenstein, M. Hansen, and A. Borrell, "The OmniTread OT-4 serpentine robot - Design and performance," *Journal of Field Robotics*, vol. 24, no. 7, pp. 601–621, 2007.
- [19] I. Walker and M. Hannan, "A novel 'elephant's trunk' robot," *1999 IEEE/ASME International Conference on Advanced Intelligent Mechatronics (Cat. No.99TH8399)*, pp. 410–415, 1999.
- [20] M. Cianchetti, A. Arienti, M. Follador, B. Mazzolai, P. Dario, and C. Laschi, "Design concept and validation of a robotic arm inspired by the octopus," *Materials Science and Engineering C*, vol. 31, no. 6, pp. 1230–1239, 2011.
- [21] M. Cianchetti, M. Follador, B. Mazzolai, P. Dario, and C. Laschi, "Design and development of a soft robotic octopus arm exploiting embodied intelligence," *Proceedings - IEEE International Conference on Robotics and Automation*, pp. 5271–5276, 2012.
- [22] K. Suzumori, S. Iikura, and H. Tanaka, "Development of flexible microactuator and its applications to robotic mechanisms," *Proceedings. 1991 IEEE International Conference on Robotics and Automation*, no. April, pp. 1622–1627, 1991.

- [23] W. McMahan, B. A. Jones, and I. D. Walker, "Design and implementation of a multi-section continuum robot: Air-octor," *2005 IEEE/RSJ International Conference on Intelligent Robots and Systems, IROS*, pp. 3345–3352, 2005.
- [24] G. Chen, M.-t. Pham, T. Redarce, and I. D. L. Villeurbanne, "Design and modeling of a silicone-based bendable tip for colonoscopy," *Tech. Rep. OCTOBER 2006*, 2006.
- [25] M. Cianchetti, T. Ranzani, G. Gerboni, I. De Falco, C. Laschi, and A. Menciassi, "STIFF-FLOP surgical manipulator: Mechanical design and experimental characterization of the single module," in *IEEE International Conference on Intelligent Robots and Systems*. IEEE, nov 2013, pp. 3576–3581.
- [26] M. D. Grissom, V. Chitrakaran, D. Dienno, M. Csencits, M. Pritts, B. Jones, W. McMahan, D. Dawson, C. Rahn, and I. Walker, "Design and experimental testing of the OctArm soft robot manipulator," no. May 2006, p. 62301F, 2006.
- [27] A. BARTOW, A. KAPADIA, and I. WALKER, "A Novel Continuum Trunk Robot Based on Contractor Muscles," *Proc. 12th WSEAS Int. Conf. on Signal Processing, Robotics, and Automation*, pp. 181–186, 2013.
- [28] M. E. Giannaccini, C. Xiang, A. Atyabi, T. Theodoridis, S. Nefti-Meziani, and S. Davis, "Novel Design of a Soft Lightweight Pneumatic Continuum Robot Arm with Decoupled Variable Stiffness and Positioning," *Soft Robotics*, vol. 00, no. 00, p. soro.2016.0066, 2017.
- [29] M. Pritts and C. Rahn, "Design of an artificial muscle continuum robot," *IEEE International Conference on Robotics and Automation, 2004. Proceedings. ICRA '04. 2004*, vol. 5, no. April, pp. 4742–4746, 2004.
- [30] G. Immega and K. Antonelli, "The KSI tentacle manipulator," *Proceedings of 1995 IEEE International Conference on Robotics and Automation*, vol. 3, pp. 3149–3154, 2002.
- [31] T. Aoki, A. Ochiai, and S. Hirose, "Study on slime robot: development of the mobile robot prototype model using bridle bellows," *IEEE International Conference on Robotics and Automation, 2004. Proceedings. ICRA '04. 2004*, no. April, pp. 2808–2813 Vol.3, 2004.
- [32] K. Kufieta, A. Waldecker, and V. Dautzenberg, "Bionic Handling Assistant," vol. 22, no. 1, pp. 6–17, 2010.
- [33] FESTO, "BionicMotionRobot Pneumatic lightweight robot with natural movement patterns BionicMotionRobot New approaches for human-robot collaboration."
- [34] D. Drotman, M. Ishida, S. Jadhav, and M. T. Tolley, "Application-driven design of soft, 3-d printed, pneumatic actuators with bellows," *IEEE/ASME Transactions on Mechatronics*, vol. 24, no. 1, pp. 78–87, 2019.
- [35] R. Maccurdy, R. Katschmann, Y. Kim, and D. Rus, "Printable hydraulics: A method for fabricating robots by 3D co-printing solids and liquids," *Proceedings - IEEE International Conference on Robotics and Automation*, vol. 2016-June, pp. 3878–3885, 2016.
- [36] W. Felt, M. J. Telleria, T. F. Allen, G. Hein, J. B. Pompa, K. Albert, and C. D. Remy, "An inductance-based sensing system for bellows-driven continuum joints in soft robots," *Autonomous Robots*, vol. 43, no. 2, pp. 435–448, 2019.
- [37] J. Zhou, X. Chen, U. Chang, J. Pan, W. Wang, and Z. Wang, "Intuitive Control of Humanoid Soft-Robotic Hand BCL-13," in *2018 IEEE-RAS 18th International Conference on Humanoid Robots (Humanoids)*. IEEE, nov 2018, pp. 314–319.
- [38] L. Chen, L. Sun, T. Yang, L. Fan, K. Huang, and Z. Xuanyuan, "RGB-T SLAM: A flexible SLAM framework by combining appearance and thermal information," *Proceedings - IEEE International Conference on Robotics and Automation*, pp. 5682–5687, 2017.